



**UNIVERSITY OF LEEDS**

This is a repository copy of *Soft robotic sleeve supports heart function*.

White Rose Research Online URL for this paper:

<http://eprints.whiterose.ac.uk/111341/>

Version: Supplemental Material

---

**Article:**

Roche, ET, Horvath, MA, Wamala, I et al. (12 more authors) (2017) Soft robotic sleeve supports heart function. *Science Translational Medicine*, 9 (373). eaaf3925. ISSN 1946-6234

<https://doi.org/10.1126/scitranslmed.aaf3925>

---

(c) 2017, American Association for the Advancement of Science. This is the author's version of the work. It is posted here by permission of the AAAS for personal use, not for redistribution. The definitive version was published in *Science Translational Medicine* Vol. 9, 18 Jan 2017, <https://doi.org/10.1126/scitranslmed.aaf3925>

**Reuse**

Unless indicated otherwise, fulltext items are protected by copyright with all rights reserved. The copyright exception in section 29 of the Copyright, Designs and Patents Act 1988 allows the making of a single copy solely for the purpose of non-commercial research or private study within the limits of fair dealing. The publisher or other rights-holder may allow further reproduction and re-use of this version - refer to the White Rose Research Online record for this item. Where records identify the publisher as the copyright holder, users can verify any specific terms of use on the publisher's website.

**Takedown**

If you consider content in White Rose Research Online to be in breach of UK law, please notify us by emailing [eprints@whiterose.ac.uk](mailto:eprints@whiterose.ac.uk) including the URL of the record and the reason for the withdrawal request.



[eprints@whiterose.ac.uk](mailto:eprints@whiterose.ac.uk)  
<https://eprints.whiterose.ac.uk/>

## Supplementary Materials for

### **Soft robotic sleeve supports heart function**

Ellen T. Roche, Markus A. Horvath, Isaac Wamala, Ali Alazmani, Sang-Eun Song, William Whyte, Zurab Machaidze, Christopher J. Payne, James C. Weaver, Gregory Fishbein, Joseph Kuebler, Nikolay V. Vasilyev, David J. Mooney, Frank A. Pigula,\* Conor J. Walsh\*

\*Corresponding author. Email: walsh@seas.harvard.edu (C.J.W.); frank.pigula@ulp.org (F.A.P.)

Published 18 January 2017, *Sci. Transl. Med.* **9**, eaaf3925 (2017)

DOI: 10.1126/scitranslmed.aaf3925

#### **The PDF file includes:**

Materials and Methods

Fig. S1. The operation of a McKibben actuator.

Fig. S2. Fabrication of PAMs with silicone bladders.

Fig. S3. Forming of thermoplastic urethane balloons.

Fig. S4. A comparison of silicone and thermoplastic urethane actuators and dynamic material properties of the actuators.

Fig. S5. Sensor fabrication.

Fig. S6. Sensing sleeve fabrication.

Fig. S7. Sensing sleeve realization.

Fig. S8. Adhesion testing.

Fig. S9. Histology from the heart after acute device use and demonstration that hydrogel interface does not affect device function.

Fig. S10. Portable power for the device, turning the device off, and peripheral perfusion in a porcine model.

Legends for movies S1 to S3

References (56, 57)

#### **Other Supplementary Material for this manuscript includes the following:**

(available at

[www.sciencetranslationalmedicine.org/cgi/content/full/9/373/eaaf3925/DC1](http://www.sciencetranslationalmedicine.org/cgi/content/full/9/373/eaaf3925/DC1))

Movie S1 (.mp4 format). Demonstration of device conformability and control scheme.

Movie S2 (.mp4 format). In vitro testing.

Movie S3 (.mp4 format). Echocardiographic data.

## **Materials and Methods**

### **Design 1 fabrication**

We used pneumatic artificial muscles (PAMs) to actuate the direct cardiac compression (DCC) device. Broadly, this class of actuators contract when pressurized with fluid. The most widely used PAM is the McKibben PAM (56, 57) (fig. S1). These actuators consist of an internal inflatable bladder enclosed in a textile mesh or braid. The mesh contracts axially when the bladder expands it radially, acting in a manner similar to a scissor linkage. We modified the fabrication process for PAMs to use silicone internal bladders for design 1, and thermoplastic urethane (TPU) bladders for design 2.

#### **Design 1 silicone actuator fabrication process**

The overall process for silicone PAMs consisted of molding silicone tubing, preparing a mesh, bonding the mesh to the tubing, and then sealing the ends. Elastomeric tubing was molded in house using a low stiffness elastomer (Ecoflex 00-30, Smooth-on, Inc.). To create the tubing, a mold was designed and 3-D printed (Objet Connex 500, Stratasys) (fig. S2A, B) and the mixed pre-polymer (part A and B of Ecoflex 00-30, Smooth-on Inc.) was injected into the mold (fig S2C) and degassed in a vacuum chamber at 10 kPa absolute vacuum for 10 minutes. Afterwards, the elastomer was cured for 1 hour in a pressure chamber heated to 60°C. A minimum outer diameter of 8 mm and wall thickness of 2 mm was chosen because molds for narrower tubing were difficult to fill using gravity alone. Before being molded over the elastomeric tubing, the mesh was locally modified to resist expansion at its ends and to prevent fraying. This was achieved by locally heating the mesh (expandable sleeving, Techflex, Inc.). The mesh was placed over a steel rod for support and the region of the tube that was not being modified was covered with heat shrink (McMaster Carr) to maintain the orientation of the fibers underneath. The end of the mesh sleeve was held to the rod with a ring of heat shrink tubing to prevent fraying when the ends were heated and compressed. The exposed mesh sleeve was compressed by sliding the two heat shrink protected areas together. When the exposed mesh was compressed, it bulged to a larger diameter, but collapsed back to the diameter of the rod when heated. After the new configuration was achieved, the fibers were allowed to cool to lock the new shape into place. After the mesh was prepared, it was bonded to the outer wall of the elastomeric tube with another layer of elastomer. This was accomplished by putting the mesh over the tube (fig S2D) and dipping both into a reservoir of mixed prepolymer, then with a heat gun (DeWalt) at maximum power at a distance of 20 cm while rotating to evenly spread and cure the elastomer. Finally, an air supply line was inserted into one end of the actuator and Sil-poxy silicone adhesive (Smooth-on Inc, USA) was placed around the airline to seal it in place. The opposite end was also sealed with Sil-poxy (Smooth-on Inc.).

#### **Characterization of silicone actuators**

The actuators were characterized to determine whether they provided the appropriate force, contraction, and rise time for use in DCC as previously described (29).

#### **Design 1 sleeve casting process**

A silicone sleeve was cast to embed oriented actuators in a cup shape using a multi-component reconfigurable 3-D printed mold. Different cores were printed with channels to accommodate actuators, and liners provided adjustability in terms of size of the cast sleeve. Sleeves with different actuator configurations were cast separately, and could be joined together afterwards. Before casting, airlines were removed from the PAMs and ends were plugged with clay. The

flexibility of the elastomer allowed airlines to be re-inserted and bonded after casting. An elastic mesh (SurgiPro, bandages.com) was used to keep actuators in place while casting. Once the actuators were aligned in the mold, the mold was assembled degassed in a vacuum chamber at 10 kPa absolute vacuum for 10 minutes, then cured in a pressure oven at 350 kPa heated to 60 °C. The circumferential and twisting layers were cast separately and integrated in a final step. Six actuators were used for the circumferential layer (three rings with two actuators per ring, allowing left and right actuation independently) and eight actuators were used for the twisting layer, oriented in a left-handed helix at an angle of 60 degrees to the horizontal.

### **Design 2 TPU actuator fabrication process**

In traditional McKibben PAMs, the bladder and mesh are crimped together at both ends to allow mechanical coupling to a load, but here we suggest decoupling one end of the braid from the bladder, allowing maximum contraction of the PAM. TPU balloons were manufactured using a thermoformer (EZform SY1217, Centroform) and a heat transfer machine (Model QX A1, Printing and heat transfer Machinery Corporation). Negative balloon half molds were 3-D printed in vero material (Objet Connex 500). Balloons were designed to be 80 mm in length (or scaled appropriately depending on location in the DCC device) with an expanded diameter of 16 mm, a shoulder of 45° and a neck inner diameter of 3.2 mm. Positive balloon halves were then molded with Dragon Skin F/X Pro (Smooth-on Inc.) using these molds.

Positive molds were placed on the vacuum platform of the heat former and a sheet of 0.25 mm TPU (Advanced Polymers Inc.) was placed in the upper heating frame of the and heated for 5 minutes at 150 °C, until the sheet sagged in the center of the heating frame, identifying that it was sufficiently heated for thermal forming (fig. S3A). Once heated the vacuum pump (Centroform) connected to the vacuum platform of the thermoformer was turned on, and the frame was carefully but quickly lowered onto the platform, causing the heated TPU to be formed around the positive molds. The sheet was allowed to cool under vacuum (15 seconds) and removed from the platform. Multiple balloon halves were fabricated from each sheet. The formed balloon halves were then trimmed so that less than 1 cm of TPU remained around the edges of the formed shape. Two formed balloon halves were placed in the negative mold and placed on the base of the heat press (fig. S3B). A sheet of polytetrafluoroethylene coated fibreglass fabric (McMaster) was placed on top of the mold to prevent the TPU from melting onto the heated platen. The two halves were sealed together using by clamping for 10 seconds at a temperature of 150°C. This process selectively applied pressure to the edges of the balloons to seal them together. The edges of the balloon were then trimmed (fig. S3C). An airline (1/8 inch OD pneumatic line, SMC corporation) was bonded to the balloon neck using Loctite 3943 (Henkel Adhesives) and UV cured for 60 seconds (fig. S3D). Braided mesh (Techflex) was cut to 115mm length and heat formed at each end. One end was closed with application of direct heat to a nut (McMaster) and placing the braid inside the nut and the other end was cut with a hot knife. The mesh was then placed over the bladder and bonded with the same UV adhesive at the airline/balloon neck interface.

### **Design 2 sleeve fabrication process**

The fabrication method for the sleeve for design 2 was a 2-D laminate process involving layering of 250 µm silicone sheets between actuator layers, and sandwiching them together in a custom designed mold before fully curing so that the layers were selectively bonded in between the PAMs. A flat mold was 3-D printed with the flat pattern of the desired sleeve, and channels where the actuators were desired. A 250 µm layer of silicone (Dragon skin F/X Pro, Smooth-on Inc.) was fabricated using an automatic film applicator (Elcometer) with a modified acrylic platform to enable larger sheet formation. The first layer of silicone was fully cured and then placed on the mold base. Then, the first layer of actuators was placed in the corresponding

grooves in the mold. The second layer of silicone was fabricated to a thickness of 200  $\mu\text{m}$ , allowed to cure, and a 50  $\mu\text{m}$  layer of uncured pre-polymer was coated on top using the automatic film applicator. This was placed on top of the first layer of actuators with the uncured polymer facing down. The second layer of actuators was then arranged on top of this layer and a third layer of silicone with a coating of uncured prepolymer (fabricated as described for layer 2) was placed on top of this assembly. The mold top was placed on this layer and the assembly was clamped and placed in the oven at 60°C. The process allowed selective welding between the silicone layers at the points that were compressed together by the mold in between the actuators. The flat configuration ensures that the sleeve is adjustable on the heart, accommodating for different heart sizes and anatomies (30).

### **Comparison of actuators for design 1 and design 2**

To compare the performance of silicone and TPU actuators four tests were conducted. The maximum pressurization of the silicone actuators before they risk failing is 10 psi, and the TPU actuator is 21 psi. The first test was measurement of maximum linear contraction, using image analysis (Image J) of screenshots from videos taken during stepwise pressurization of each actuator (fig. S4A). The second test was to measure linear force generation at maximum pressurization. Samples were mounted in a mechanical tester (Instron 5566, Instron), and actuated cyclically to maximum pressure at a rate of 1 Hz with a 200 ms actuation period. A peak detection algorithm was used to find the first ten peaks, and these were averaged for all samples to obtain the maximum linear force (fig. S4B). The third test measured the reduction in cross-sectional area of silicone discs representing cross-sections of the heart at the apex, middle and base. Areas were calculated using Image Analysis (Image J) (30) (fig. S4C). Finally the fourth test measured the force generated by a ring made up of two actuators mounted onto a clamshell test fixture (fig. S4D). This is representative of the circumferential actuators in the device. Testing was carried out as described for the linear force generation, except a fixture was mounted in the upper and lower clamps, and the ring actuator was positioned around the appropriate groove in the fixture before cyclical actuation.

As shown in fig. S4 the TPU actuators out-performed the silicone actuators in terms of linear contraction and force generation (fig. S4 A,B) and circumferential area reduction and force generation (fig. S4 C,D). These actuators were incorporated into design 2.

### **Characterization of the dynamic properties of the PAMs**

We conducted experiments on the pressurized PAMs to compare to literature values for active cardiac muscle as follows;

Isometric testing: The PAM was held at a fixed distance in the mechanical tester and pressurized to 12 psi for 500 ms, then depressurized (fig. S4E). This was repeated ten times for  $n = 3$  PAMs, A representative graph showing engineering stress vs time is shown in fig. S4F.

Isotonic testing: We conducted isotonic (constant pressure) testing to generate a stress/strain curve. The PAM was pressurized to 12 psi and held at that constant pressure. The crosshead of the mechanical tester was adjusted until a zero force was registered, and the gauge length was reset to 0. Then the pressurized PAM was tested in tension (fig. S4G). The force/displacement curve was recorded, and then converted to an engineering stress/strain curve by dividing the force values by the initial cross-sectional area ( $A_0$ ) and the displacement values by the initial length ( $L_0$ ) (fig. S4H). Although the overall curve had viscoelastic properties, for comparison to literature values of Young's modulus, the slope of the initial linear part was calculated as the Young's modulus for the first 5% of strain. The pressurized PAM was then tested in compression by returning the crosshead to a zero load. A compressive modulus was calculated as the slope of

the compressive stress/strain curve. We calculated the modulus as ~560 kPa for the first 5% tensile strain and the compressive modulus as ~595 kPa.

### **Sensing sleeve fabrication**

A detailed description of the sensing sleeve fabrication has been previously described (31). To create a stretchable, conformable, yet robust circuit that ensures the power supply and communication with multiple sensors, we used barometric sensors in a stretchable 500  $\mu\text{m}$  silicone layer from Dragon Skin F/X Pro (Smooth-on Inc.). A barometric sensor was mounted on a double sided printed circuit board (PCB) (fig. S5A) which allowed the essential pin connections and capacitor fixations for a robust digital communication on one side while enabling proximal fixation to the circuit of the readout electronics on the other side. This eliminated having vulnerable electrical connections on the edges of the sensor/PCB assembly and minimized bending and potential damage to electronic connections during use. The barometer/PCB assembly was centered in a 3-D printed mold with a reservoir (fig. S5B) to degas, while preventing any material loss. Urethane rubber (Vytaflex 40, Smooth-on Inc.) was poured into the mold and degassed with 100 kPa gage vacuum for five minutes. Subsequently the assembly was cured at 80 kPa gage vacuum (fig. S5C) at 20 °C for 24 hours without removing it from the vacuum chamber so that the barometer diaphragm slightly relaxed, thereby increasing the functional range of the resulting sensor. We designed a multi-part fabrication tool to allow transfer printing of an array of interconnected sensors onto a flexible silicone layer (fig S6A). The tool is comprised of three sheets: sheet 1 is the wire-wrapping sheet, sheet 2 the transfer printing sheet, and sheet 3 the sensor alignment sheet. Sheet 3 allows placement of sensors in the desired configuration for the DCC device, sheet 2 allows lifting and transfer of the entire circuit and sheet 1 allows positioning of circuitry wire in a stretchable configuration considering the actuator design of the DCC device. We used flexible flat cables (FFC) for communication between the sleeve and the processing unit. The interconnection scheme was designed to mimic features of the DCC device and so that the circuit connections would experience the least amount of strain when on the beating heart.

Sheets 1 and 2 were assembled and magnet wire was continuously wrapped around the alignment fixtures in a meandering pattern (fig. S6B). Wires were wrapped so they passed over the sensor space-holders. Up to 24 sensors were manufactured and positioned, PCB side down, in sheet 3 then placed onto the subassembly of sheets 1 and 2. Wrapped wires were spot-soldered from the bottom side of the assembly. This was repeated for a total of five connections per sensor; power (VCC), ground (GND), data line (SDA), clock line (SCL) and a chip select line (CS). To ensure sensor array functionality during malfunction of a single sensor the four supply and communication lines (VCC, GND, SDA, SCL) are shared among multiple sensors and were fabricated from continuous wires. As multiple Microelectromechanical systems (MEMS) barometric sensors cannot be addressed individually by the Inter-Integrated Circuit ( $I^2C$ ) bus for read out, one chip-select (CS) line was connected to each sensor to avoid on/off switching during usage and thereby not impede the sampling rate. Sheet 2 was lifted from the wire alignment sheet with the entire circuitry (sensor array with wires) (fig. S6C). This flat configuration allowed the circuit to be transferred on to a 250  $\mu\text{m}$  silicone sheet (fabricated using an automatic film application, Elcometer). The circuit was pressed onto the silicone and sheet 2 was removed. PCBs were protected by vapor deposition coating of 25  $\mu\text{m}$  Parylene C (Specialty Coating Systems Inc.). Finally, a second layer of 200  $\mu\text{m}$  thick silicone (Dragon skin F/X Pro, Smooth-on Inc.) was coated with a 50  $\mu\text{m}$  uncured layer of prepolymer, and placed on top of the silicone/circuit assembly (fig. S6D). Pressure was applied to the sheets in between the sensors and the silicone was allowed to cure at room temperature. The sleeve was trimmed to match the geometry of the DCC device (fig S6D). The resulting sensor and sensing sleeve are shown in fig.

S7A and B. Fig. S7C shows how the sleeve can conform to the surface of a porcine heart and fig. S7D shows the sleeve with the DCC device.

### **Control box**

A custom software interface was developed (Labview, National Instruments), allowing simultaneous data acquisition and device control (200 Hz) with an X-Series DAQ card (National Instruments). Clinical parameters (ECG, pressures, flow) were read from clinical monitoring equipment and raw analogue input signals were converted into engineering units (e.g. L/min, mmHg) and visually displayed in waveform charts on the user-interface. Data was logged allowing post-processing analysis of device performance. The hardware was mounted in a portable case for bringing to animal trials. The system used wall compressed air and vacuum. The fluidic-control hardware consisted of two electro-pneumatic regulators (ITV series, SMC Corporation) and sixteen independent solenoid valves (high-flow 3-way VQ series, SMC corporation) to allow independent pressurization of each actuator.

### **Fixation on heart**

For both designs, a suction device (Starfish heart positioner, Medtronic) was incorporated into the device via a laser-cut acrylic ring, through which the airlines from the twisting actuators were placed with a clearance fit. The ring was fixed around the base of the Starfish, so that there was an inbuilt suction cup on the device for fixation, stabilization and transmission of torsion at the apex of the heart. However, fixation to the base of the heart was challenging. We tested four methods of adhesion to the heart: a custom-made suction strip using multiple suction cups; a grip layer (3M) attached to a silicone strip; silicone with small holes (formed by a 2 mm biopsy punch) in combination with cyanoacrylate (3M); and finally medical mesh (Fix-pro, Bandages Plus) with cyanoacrylate adhesive. A freshly explanted porcine heart was mounted into a custom-made test fixture, and fixed in the lower clamp of a mechanical tester (Instron 5566) (fig S8A). Each adhesion method was attached to the base of the heart in turn, and then attached to pull-wires mounted in the upper crosshead (1 m gauge length) using binder clips. The strips (fig. S8B) were pulled off at 100 mm/min and the maximum force was recorded for each group ( $n = 3$  strips). The adhesion testing demonstrated that the strongest adhesion to fresh heart tissue was with cyanoacrylate adhesive. Fig. S8C shows an adhesion force of up to 16 N for adhesive with mesh or silicone at the heart/tissue interface. Cyanoacrylate was used in our in vivo trials as a temporary fixation method.

### **Evaluation of the effect of hydrogel on device efficacy**

To determine whether the device efficacy is affected by alginate polyacrylamide hydrogel at the device-tissue interface we measured the force transmitted by a circumferential actuator with a fixture similar to the clamshell fixture in fig. S4C. We conducted measurements for 1 minute each for the following conditions: (i) without the hydrogel, (ii) with the hydrogel, and (iii) with the hydrogel after 2,300 cycles continuous compression at a pressure of 21 psi and a frequency of 1 Hz for 200 ms actuation periods. A graph of the average cyclical maximum force is shown in fig. S9B. The force increases slightly with the hydrogel, and doesn't decrease after continuous cycling.

### **Ex vivo imaging**

We conducted computed tomography imaging to visualize the conformation of the device to the heart. An X-ray Micro-computed tomography system (Nikon Metrology (X-Tek) HMXST225 MicroCT) and a 1621 X-ray panel (Perkin Elmer) was used to generate the clinical images. The work was carried out at the Harvard Centre for Nanoscale Systems. The following settings were used: a 0.5mm copper filter, voltage of 120 kV, current of 88 uA, focus -27, exposure time per

image 5 seconds and scan time 30 minutes. Reconstruction was carried out with VGStudio MAX and FEI's Avizo 3D software.

### **In vivo testing**

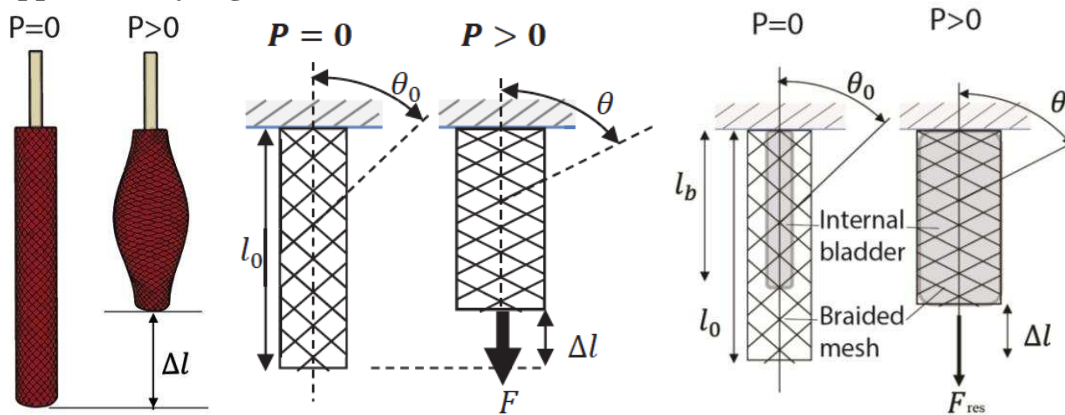
All animals were acclimatized in the holding facilities for at least a day before the initiation of each study. Food, but not water was withheld for 14 to 16 hours before sedation and induction of anaesthesia. Anaesthesia was induced with tiletamine/zolazepam HCl (Telazol, 4.5 mg/kg, Zoetis), xylazine (2 mg/kg, Akorn animal house), and atropine (0.04 mg/Kg intramuscularly, West-ward). Anaesthesia was maintained with isoflurane (0.5% to 1%, Baxter) and oxygen. Animals were intubated after induction, and placed on mechanical ventilation using volume-cycled ventilation at 10 mL/kg at a rate of 10-20 breaths/min. Inhalant anesthetics were delivered. When animals were stabilized a femoral venous and arterial line were placed percutaneously using the Seldinger approach. A jugular catheter (Veterinary Central Venous Catheter Set, Ref CVS50IJ, Surgivet) was then introduced and secured. Baseline in-vivo control data was recorded for 5 minutes. Lidocaine was administered prophylactically to reduce the risk of ventricular arrhythmias caused by the placement and attachment of the DCC device. Lidocaine was administered by a bolus intravenous (IV) injection dose ranging from 0.5–0.75 mg/kg and up to 1–1.5 mg/kg (about 50–100 mg) was administered at a rate of approximately 25–50 mg/minute (0.35–0.7 mg/kg per minute). An IV infusion at a rate of 20–50 mg/kg per minute was then administered. If the desired response was not achieved an additional bolus dose of 0.5–0.75 mg/kg as a rapid intravenous (IV) injection was repeated at 5- to 10-minute intervals as necessary, up to a total dose of 3 mg/kg. Unfractionated heparin (300 iu/Kg IV, Hospira) was administered prophylactically to reduce the risk of venous thromboembolism during the procedure. Monitoring during the procedure included continuous ECG tracings, arterial blood pressure and central venous blood pressure through femoral lines, intra-ventricular pressures, pulmonary and aortic flow rates, peripheral capillary oxygen saturation (SpO<sub>2</sub>) percentage. Echocardiography was used to determine anatomical and physiological data including the size and shape of the heart, pumping capacity. A sternotomy was used for access. A paralytic agent (cisatracurium besylate, 0.1-0.4mg/kg IV) was administered to facilitate sternotomy and avoid excessive muscular fasciculations, which could lead to blood loss. The animal was instrumented with an ultrasonic flow probe on the aorta and pulmonary trunk (16PS and 20PS, Transonics Inc.) connected to a T402 multi-channel research console (Transonics Inc.). The left atrium and pulmonary artery were cannulated with 26G catheters and a pressure sensor (Surgivet Inc.) was attached to each catheter. ECG and pressure data was logged to the DAQ via a 9-pin analog connector (Digikey) connected from a Surgivet Vital signs monitor set to run on label-switch interval (LSI) protocol. Flow data was logged using Bayonet Neill–Concelman (BNC) connectors (Digikey). After instrumentation and establishing a stable hemodynamic condition, five minutes of baseline data was recorded to measure cardiac performance. Epicardial pacing was used to control the heart rate, if necessary, to help with device synchronization. To evaluate the effects of the DCC devices on the acutely failing heart, acute heart failure was pharmacologically induced by using a short acting  $\beta$ -blockade, esmolol (Mylan) to reduce contractility of the heart and lower cardiac output in a dose-dependent manner. Esmolol was infused intravenously at a rate of 0.15 – 1 mg/kg/min and supplemented by bolus injections of 0.5–1 mg/kg as needed to achieve effect. With the induction of this model, heart rate (and as a result cardiac output) decreases. After hemodynamics stabilized, another baseline data recording was taken for five minutes. The device was placed on the heart and affixed using the active suction cup at the apex, and mechanical fixation at the base (sutures, velcro or adhesive). While the device can be triggered from ECG, we largely triggered it from a pacemaker signal while the heart was being paced due to the failing status of the heart or severe bradycardia from esmolol. Device parameters (actuation period, delay and speed) could be adjusted. By using a dual

chamber pacemaker (5342, Medtronic Inc.), the delay could be fine-tuned manually. Data was continuously logged during the entire trial. At the end of the trial (maximum length was four hours), the animal was euthanized by an intra-venous injection of sodium pentobarbitol (Fatal-Plus, 110mg/kg, Baxter).

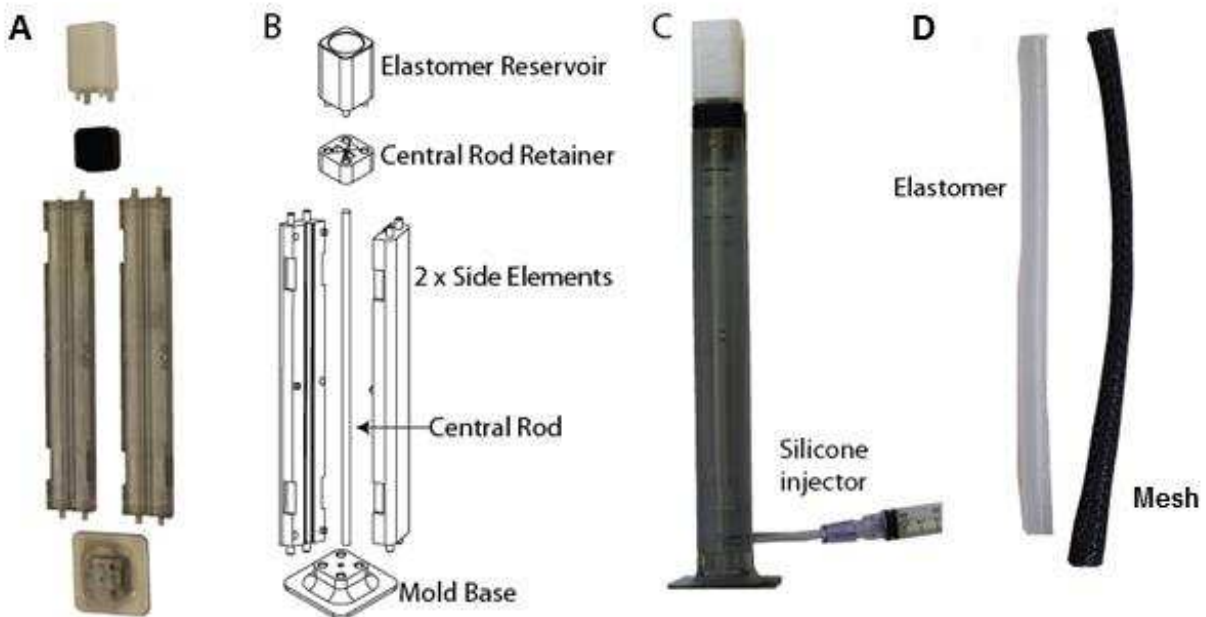
### **In vivo imaging**

Image acquisition was performed using the Philips IE33 ultrasound machine using an X7-2t probe. Three measurements of the mitral inflow E wave and tissue Doppler lateral mitral valve annulus E' were obtained and averaged for each condition. The E/E' ratio was then calculated as a measure of diastolic function. 3D full volume acquisitions were obtained over 4 consecutive beats. LV volumes and twist were calculated using a commercial 3D speckle-tracking analysis package (4D LV Analysis 3.1, Tomtec Imaging Systems).

Supplementary Figures

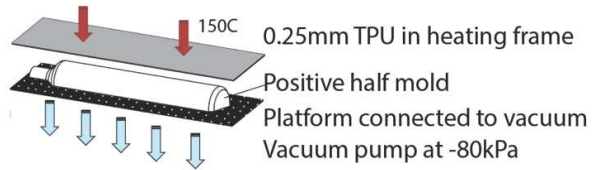


**Fig. S1: The operation of a McKibben actuator.** The internal bladder can be coupled to both ends of the mesh, or decoupled from one end of the mesh.  $P$  = pressure,  $l$  = length,  $l_0$  = initial length,  $l_b$  = balloon length,  $\Theta$  = braid angle.



**Fig. S2: Fabrication of PAMs with silicone bladders.** (A) 3-D printed mold. (B) Drawing of mold parts. (C) Elastomer being injected into the mold. (D) Molded silicone tube and braided mesh with locally modified ends.

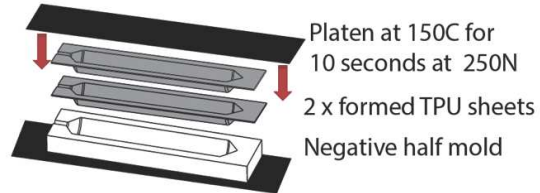
A Thermo-form each balloon half



C Trim edges



B Heat seal halves together



D Attach airline,inflate

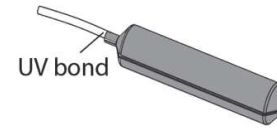


**Fig. S3: Forming of thermoplastic urethane balloons.** (A) A thermoformer was used to form balloons at 150°C with -80 kPa vacuum and 250 N force. (B) Two formed balloon actuator halves were sealed together using a heat press. (C) The edges were manually trimmed. (D) The airline was UV bonded to balloon neck and balloon was inflated. UV = ultra-violet

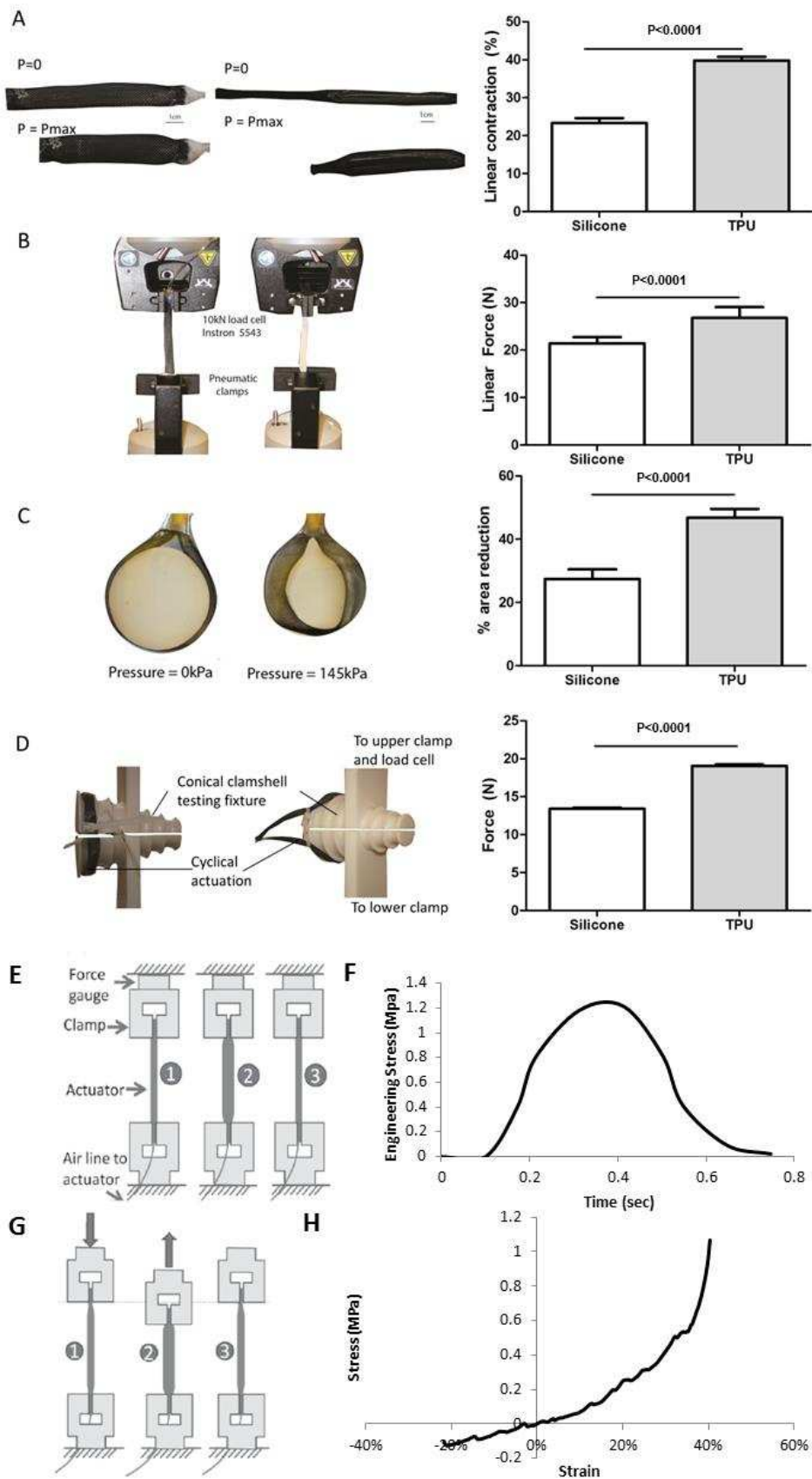


**Fig. S4: A comparison of silicone and thermoplastic urethane actuators and dynamic material properties of the actuators. (A) Linear contraction of both types of actuators in %.  $P =$**

pressure **(B)** Linear force generation for both actuators at maximum pressure. **(C)** The % area reduction of a cylindrical disc with a diameter approximating that of the apex. Reduction occurs due to a change in pressure. **(D)** Force generation from a ring configuration of two actuators in silicone and TPU. For all tests, data are mean+SD ( $n = 10$ ), using an unpaired 2-tailed t-test, with a confidence interval of 95%. **(E)** Isometric test set-up. The PAM was held at a fixed distance (1), pressurized to 12 psi for 500 ms (2), then depressurized (3). **(F)** Dynamic change of stress over one pressurization cycle. The graph shows a representative graph from  $n = 3$  PAMs cycled 10 times. **(G)** Isotonic testing set-up. The PAM was pressurized to 12 psi and held at that constant pressure (1); the crosshead of the mechanical tester was adjusted until a zero force was registered, and the gauge length was reset to 0 (2); then the pressurized PAM was tested in tension (3). **(H)** Stress/strain curve for the PAMs. The graph is representative of  $n = 3$  PAMs tested.

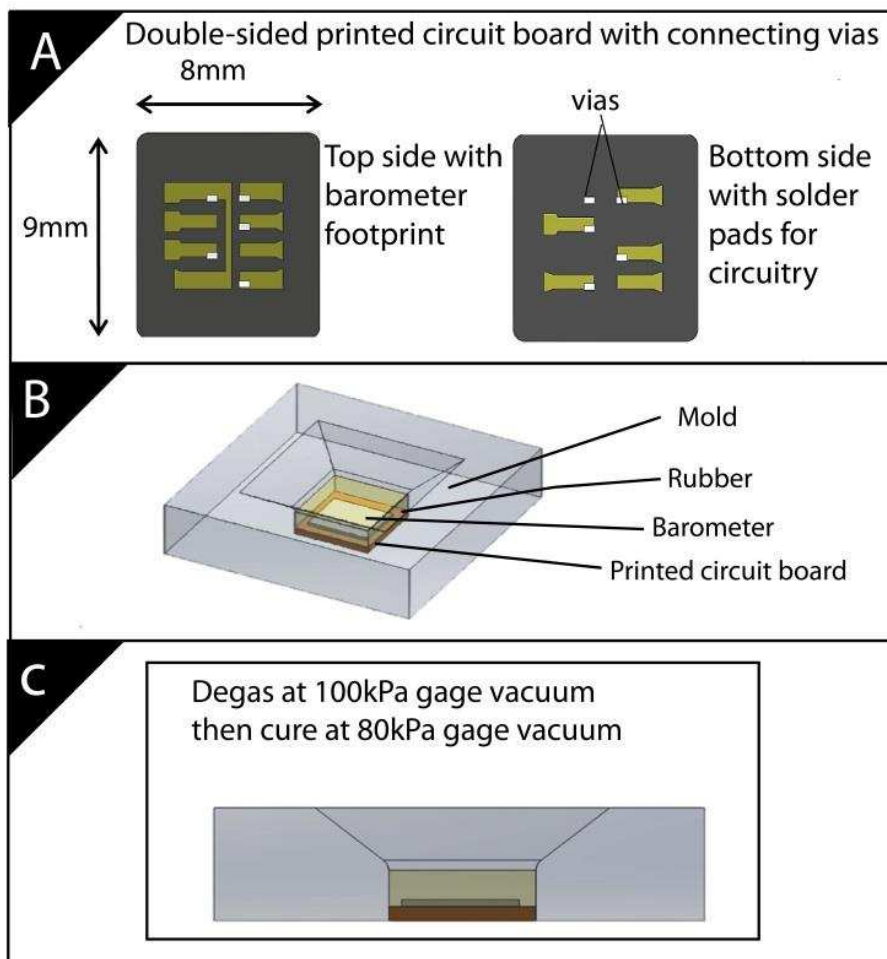


**Fig. S5: Sensor fabrication.** (A) Double-sided printed circuit board (PCB) designed to protect electrical connections. (B) Mold with reservoir for casting of barometer/PCB assembly with rubber. (C) Assembly is degassed at 100kPa gage vacuum and cured at 80 kPa gage vacuum.

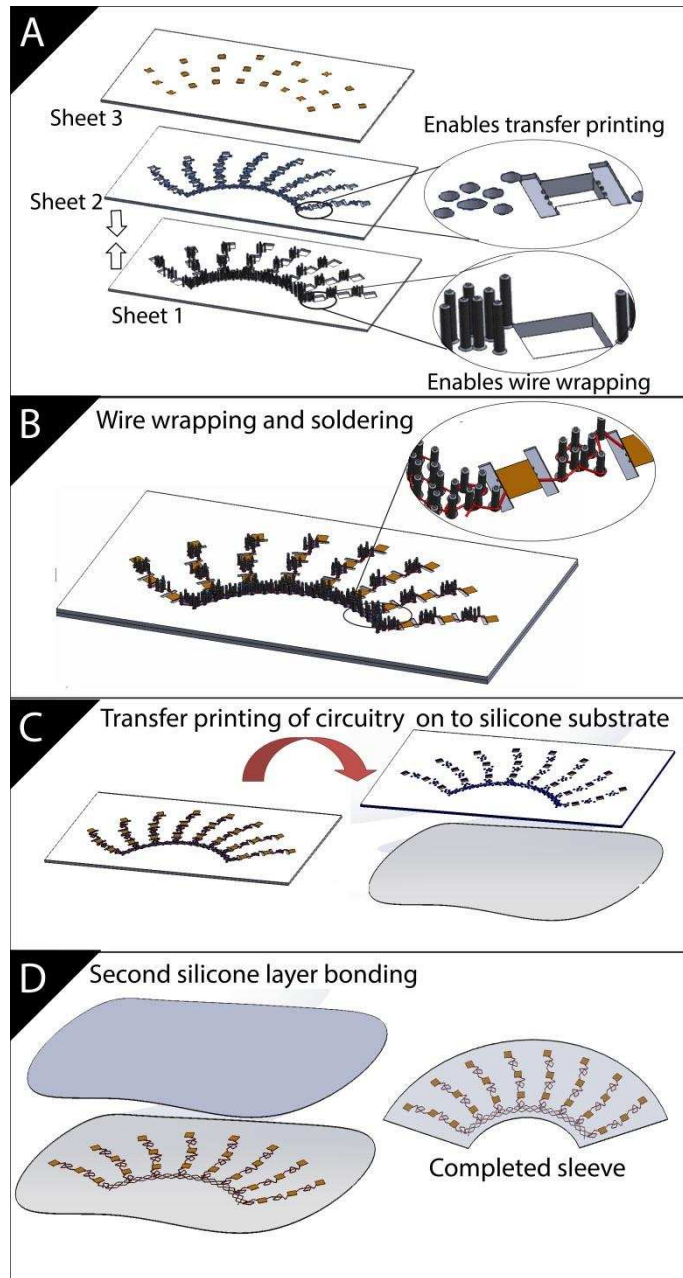


**Fig. S6: Sensing sleeve fabrication.** (A) A multi-sheet fabrication tool allows transfer printing of circuitry onto a flexible silicone layer. Sheet 3 is used to position an array of sensors on to an assembly of sheet 1 and sheet 2. (B) Sheet 1 and 2 were assembled, and wires were wrapped around posts from sheet 1. Sheet 3 was used to place sensors, and then removed. Wires were soldered to sensors in-place, and wire wrapping was repeated for each of five lines. (C) After wrapping, sheet 2 can be lifted off so that the assembly and all circuitry (sensors and interconnecting wires) can be transferred to a thin ( $250\ \mu\text{m}$ ) silicone sheet. (D) A second silicone sheet coated with  $50\ \mu\text{m}$  of uncured prepolymer is transferred onto assembly and cured with selective pressure between sensors, and then completed sleeve is trimmed to size.

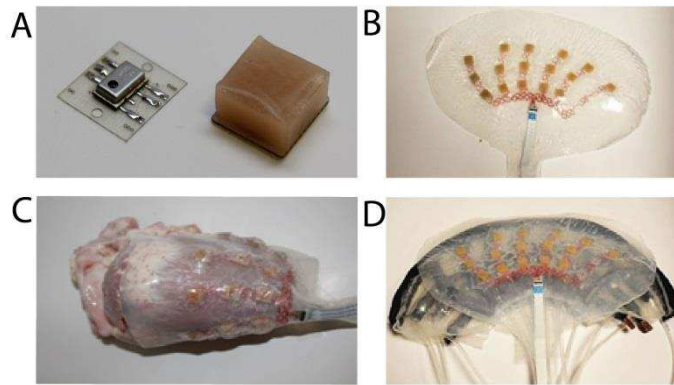


**Fig. S7: Sensing sleeve realization.** (A) Microelectrical mechanical systems (MEMS) barometer on a double-sided PCB alongside sensor cast in urethane rubber. (B) Final sensing sleeve. (C) Sensing sleeve conforming to heart (D) Sensing sleeve aligned with DCC device.

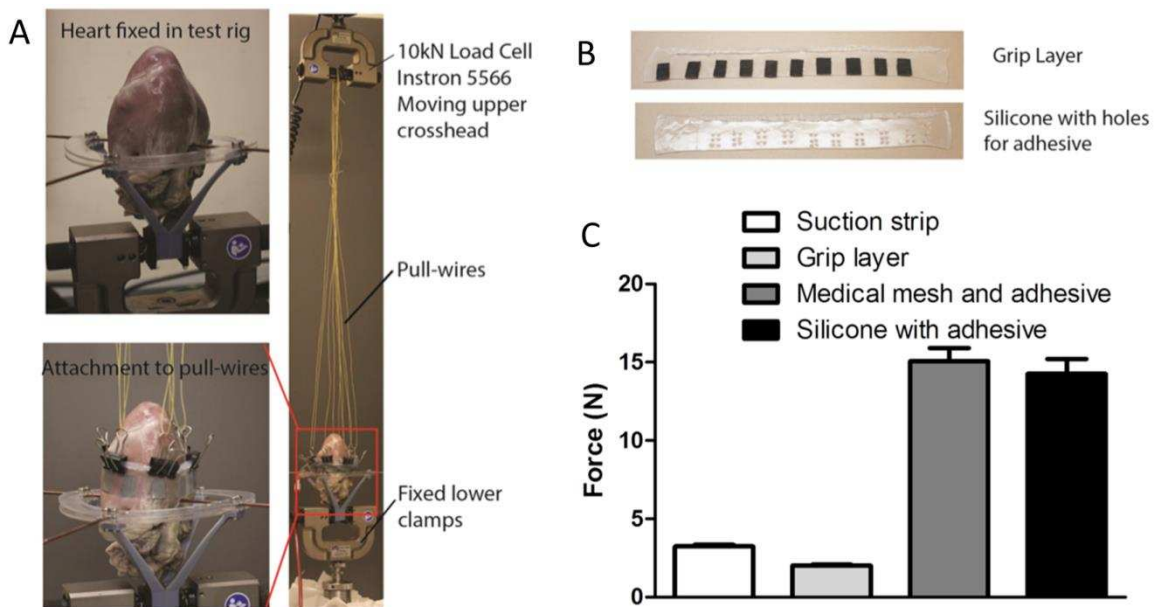


**Fig. S8: Adhesion testing.** (A) Adhesion test set-up. A freshly explanted porcine heart was mounted in a custom-made test fixture, and fixed in the lower clamps of a mechanical tester. Fixation options were attached to the base of the heart, and connected to pull-wires by clamps attached to a thicker rim of silicone on the strip. The strips were pulled off and maximum force was recorded. (B) Grip layer and layer of silicone with adhesive. (C) Adhesion testing shows that use of cyanoacrylate adhesive provides best adhesion to the heart. Data are means + SD (n = 3).

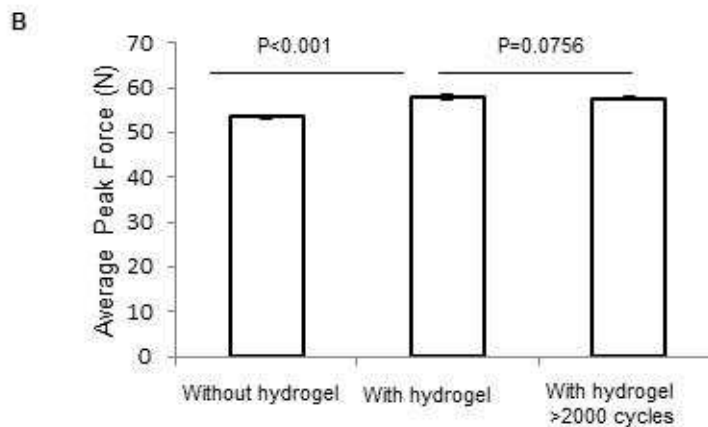
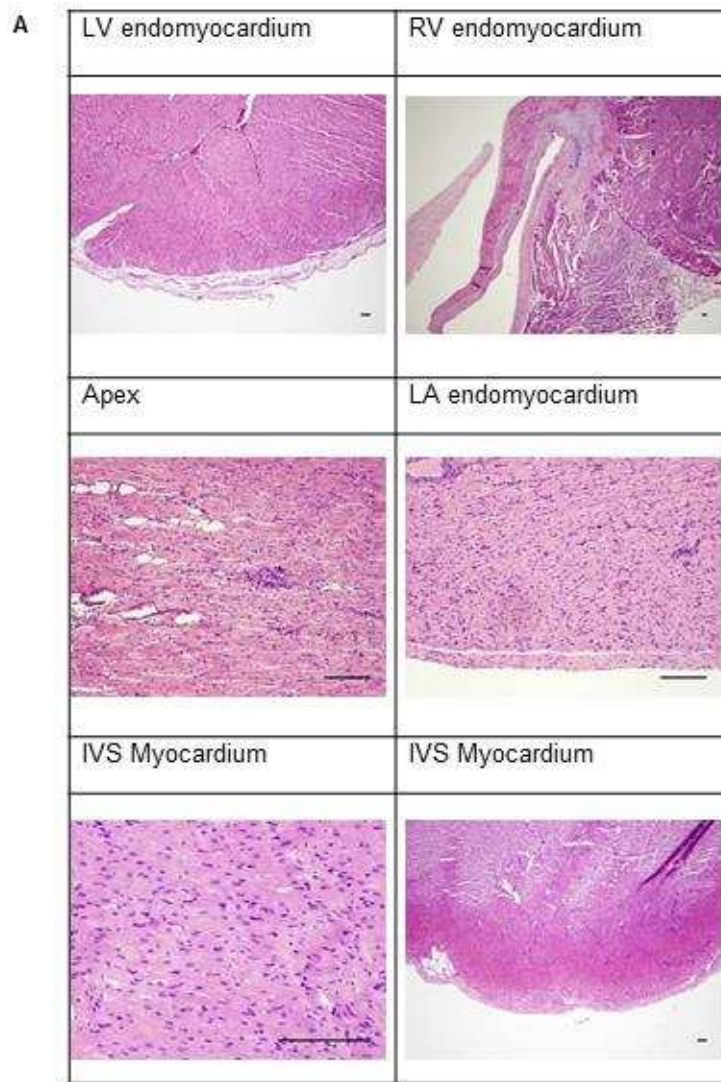


**Fig. S9: Histology from the heart after acute device use and demonstration that hydrogel interface does not affect device function.** (A) Hematoxylin–eosin-stained paraffin-embedded sections from porcine heart after two hours of actuation. LV = left ventricle, LA = left atrium, IVS = intraventricular septum. Scale bar = 125 $\mu$ m. (B) Average cyclical maximum force for each of the conditions (i) without hydrogel, (ii) with hydrogel and (iii) with hydrogel after more than 2000 cycles. Data are mean  $\pm$  standard deviation, 1-way ANOVA, 60 cycles of data were collected for 1 PAM in each condition.

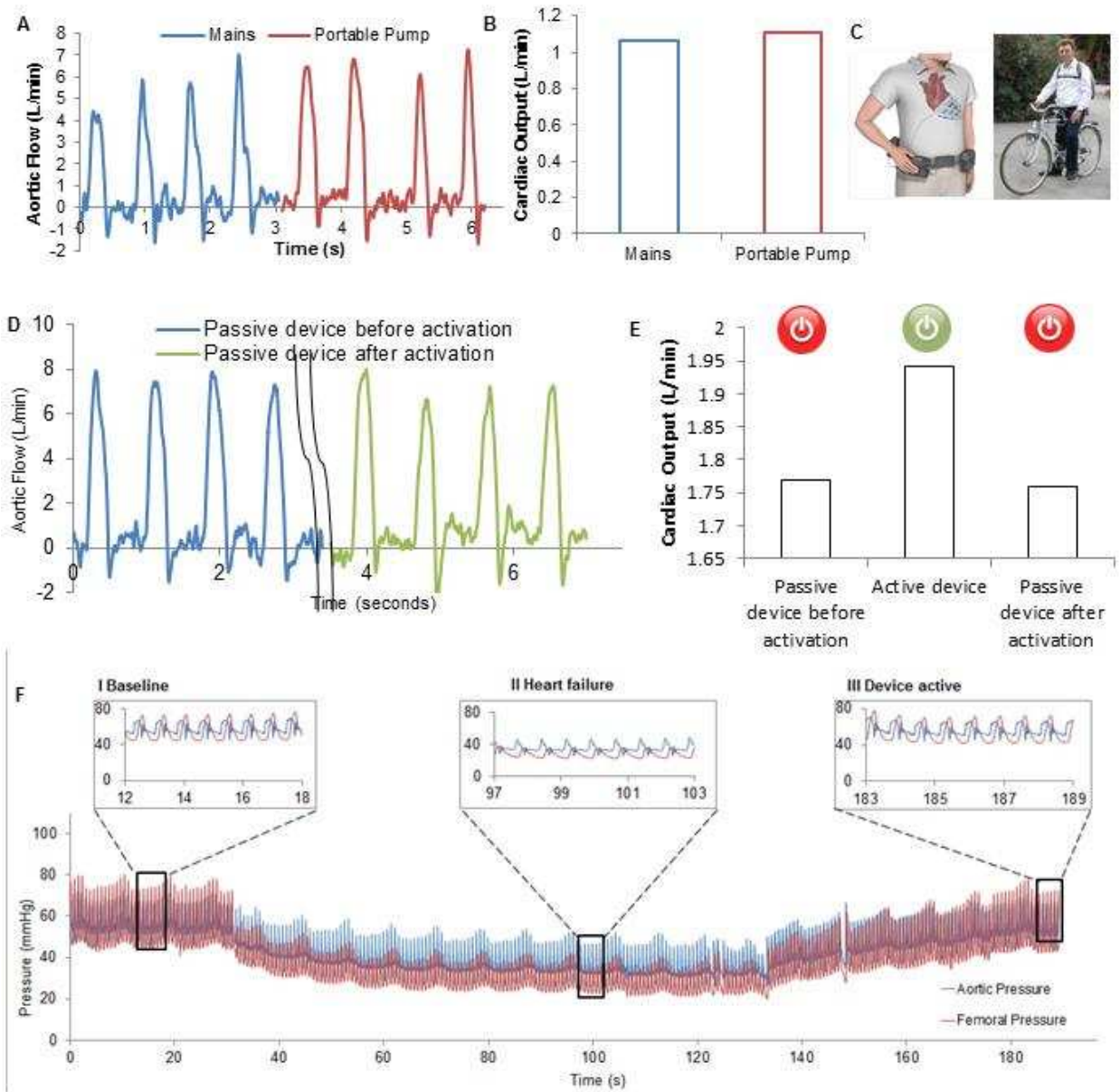


**Fig. S10: Portable power for the device, turning the device off, and peripheral perfusion in a porcine model. (A)** Aortic flow for four representative samples when powered with the mains and a portable pump. **(B)** Cardiac output (average aortic flow for 10 cycles) for each condition. **(C)** Envisioned carrier for pump, and predicate backpack for air canister (reproduced with permission from Syncardia). **(D)** Aortic flow for four representative cycles with the passive device before and after activation **(E)** Cardiac output (average aortic flow for 10 cycles) for each condition. **(F)** Aortic and peripheral (femoral) pressures for baseline, heart failure and when the device is active.

## **Supplementary Movies**

### **Movie S1: Demonstration of device conformability and control scheme**

The movie shows video footage and 2D and 3D echocardiographic videos of the device (circumferential actuators only) on the porcine arrested heart. The conformability can be clearly visualized as the device moves with the heart tissue. The control capabilities are then highlighted by showing simultaneous, sequential and twisting actuation of the device on an arrested porcine heart.

### **Movie S2: In vitro testing**

This movie shows the in vitro testing corresponding to Fig. 3 in the manuscript. The device in different configurations is shown on the univentricular in vitro model, with blue lines indicating the maximum fluid volume displacement for that configuration. A device with silicone actuators (left) was compared to a similar device with TPU actuators (right). The 2D lamination process described in the text was used for both devices used in this video, to allow a direct comparison. For each device, either the circumferential layer or the twisting layer was placed on the outside as can be seen in the video. Device 1 is then shown on the biventricular in vitro model demonstrating a separate volumetric output from each ventricle of the model.

### **Movie S3: Echocardiographic data**

This movie shows echocardiographic and Doppler videos from 2 pigs when the device is actuated (device on) and unactuated (device off) on the heart.